Band-Gap Engineering: From Physics and Materials to New Semiconductor Devices

FEDERICO CAPASSO

Band-gap engineering is a powerful technique for the design of new semiconductor materials and devices. Heterojunctions and modern growth techniques, such as molecular beam epitaxy, allow band diagrams with nearly arbitrary and continuous band-gap variations to be made. The transport properties of electrons and holes can be independently and continuously tuned for a given application. A new generation of devices with unique capabilities, ranging from solid-state photomultipliers to resonant tunneling transistors, is emerging from this approach.

IN RECENT YEARS THERE HAS BEEN AN INTENSE RESEARCH effort on semiconductor heterojunctions. This field is an excellent example of how basic science and technology interact and influence one another.

Early suggestions for using semiconductor heterojunctions to improve device performance are found in the celebrated transistor patent of Shockley (*1*). A few years later, Kroemer (*2*) proposed the concept of a compositionally graded semiconductor. By spatially varying the stoichiometry of a semiconductor, an energy band gap is produced that varies with position (graded band gap). Thus "quasi-electric forces," equal to the spatial gradient of the conduction and valence band edge, respectively, are exerted on the electrons and holes. This concept is one of the earliest and simplest examples of band-gap engineering, which is the spatial tailoring of the band gap or, more generally, the band structure of a semiconductor to achieve new material and device properties (*3*).

After the initial demonstrations of the homojunction semiconductor injection laser in the early 1960's, Kroemer suggested that carrier confinement in a low-gap region clad by wide-gap heterojunction barriers would make population inversion and laser action possible at much lower current densities (*4*). The demonstration of a continuous wave (CW) heterojunction laser at 300 K (*5*) was made possible by the growth of high-quality AlGaAs/GaAs heterojunctions by liquid phase epitaxy and paved the way to high-performance lasers for lightwave communications.

The next breakthrough was the invention of molecular beam epitaxy (MBE) at Bell Laboratories by Cho and Arthur (*6*). This epitaxial growth technique allows multilayer heterojunction structures to be grown with atomically abrupt interfaces and precisely controlled compositional and doping profiles over distances as short as a few tens of angstroms. Such structures include quantum wells, which are a key building block of band-gap engineering. These potential energy wells are formed by sandwiching an ultrathin lower gap layer (of thickness comparable or smaller than the carrier thermal de Broglie wavelength, which is $\approx$250 Å for electrons in GaAs) between two wide-gap semiconductors (for example, AlGaAs). The spacing and position of the discrete energy levels in the well depend on the well thickness and depth (*6*). The well depth is the energy difference between the bottom of the conduction bands (or the valence bands in the case of holes) in the two materials and is also termed band discontinuity. Band discontinuities play a central role in the design of heterojunction devices such as quantum well lasers (*7*). These lasers have important applications in the area of optical recording.

If many quantum wells are grown on top of one another and the barriers are made so thin (typically <50 Å) that tunneling between the coupled wells becomes important, a superlattice is formed. This concept was first proposed by Esaki and Tsu at IBM in 1969 (*8*). It has since attracted a tremendous interest, which was spurred by the development and the unique capabilities of MBE and other growth techniques such as metallo-organic chemical vapor deposition (MOCVD) (*9*). Superlattices are new materials with novel optical and transport properties introduced by the artificial periodicity. Other superlattices with intriguing properties can be obtained by periodically alternating ultrathin *n*- and *p*-type layers [nipi (*n*-type intrinsic *p*-type intrinsic) superlattices] (*10*), by periodically grading the composition (sawtooth superlattices) (*11*), or by alternating undoped layers with doped layers that have a wider band gap (modulation-doped superlattices) (*12*). Modulation doping in a single heterojunction is the key element of a new high electron mobility transistor (*13*). Strained layer superlattices have also shown interesting properties and have potential as components of new devices (*14*).

The rich variety of available combinations of band gaps, semiconductor alloys, and lattice constants is the main feature of band-gap engineering (*15, 16*). A few years ago, I realized that the ability to engineer the band diagram of a semiconductor structure in an almost arbitrary and continuous way opened the door to exciting possibilities for optical detectors and other devices. These are reviewed here.

Solid-State Photomultipliers and Graded Gap Transistors

When light strikes a semiconductor, it is absorbed if the energy of the photons exceeds a threshold, the energy band gap, which has different characteristic values for different semiconductors. In a photodetector, electrons in the valence band (bound electrons) that gain enough energy by absorbing incident photons can cross the band gap into the conduction band and become free electrons. An applied external voltage or the electric field of a *pn* junction spatially

The author is a Distinguished Member of Technical Staff at AT&T Bell Laboratories, Murray Hill, NJ 07974.

Fig. 1. Band-gap engineering applied to avalanche photodiodes (APD's). (**a**) Multiquantum well APD; (**b**) solid-state photomultiplier (staircase APD); and (**c**) channeling APD.

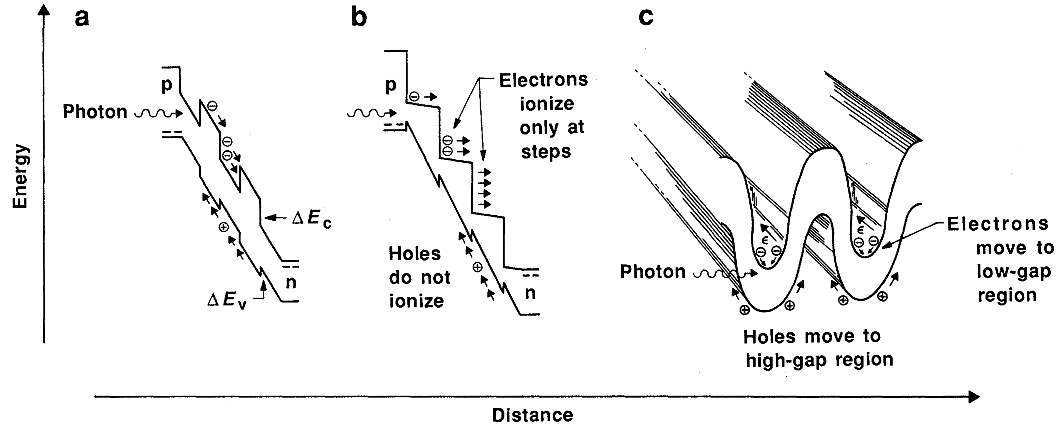

separates the free electrons and holes that photons generate, so that they can be routed to the external circuit. This process can be simply represented with an energy-band diagram, in which the vertical axis represents energy and the horizontal axis shows distance inside the semiconductor (Fig. 1). The electric field "tilts" the energy bands, so that electrons generated by photons drift "downhill" to the lower edge of the conduction band and holes ascend to the upper edge of the valence band. The composition and the doping of the semiconductor can be tailored so that band diagrams with nearly arbitrary band-gap variations and shapes can be synthesized (band-gap engineering).

The avalanche photodiode (APD), a special type of *pn* junction photodiode, can greatly enhance the electrical signal. Its name comes from the avalanche-multiplication process, analogous to rocks rolling down a mountain and dislodging more rocks, that amplifies the signal. In an APD, the photoinjected carriers (electrons or holes or both) gain energy from the electric field and undergo ionizing collisions (impact-ionization) with the atoms of the lattice. These collisions create more carriers across the forbidden band gap, which in turn impact-ionize other atoms and so on. The minimum energy required to create an electron-hole pair by an ionizing collision is called the ionization threshold energy. This energy is greater than the band gap.

Low-noise operation is important if an APD is to detect the low power levels of signals that emerge from long distances in optical fibers. Avalanche multiplication, however, generates extra noise, which adds to the shot noise of the incident photons. This so-called excess noise arises from the fluctuations of the avalanche gain. Avalanche multiplication occurs in two directions, since holes and electrons travel in opposite directions. If both electrons and holes undergo ionizing collisions at nearly the same rate, the avalanche is equally strong in both directions. Any slight fluctuation (a variation in the number of carriers created) in the electron-multiplication process is immediately fed back and amplified because of hole-initiated impact-ionization. This feedback strongly reinforces the original fluctuation so that the excess noise is very large. If only one type of carrier can ionize, however, the avalanche proceeds in only one direction. As a result, the avalanche-feedback process does not occur and excess noise is reduced.

To limit the excess noise caused by the avalanche, holes and electrons must ionize at vastly different rates. Ideally, one of the ionization rates should be zero, but no materials have that desirable characteristic. In silicon the ratio of these ionization rates (one rate for electrons, α, the other for holes, β) is greater than 20 to 1, so there is little avalanche noise. But silicon is not sensitive at wavelengths that fall in the low-loss, low-dispersion, long-wavelength region of optical fibers (1.3 to 1.6 μm). For this spectral region, no material currently can match the noise performance of silicon at shorter wavelengths; virtually all III-V materials (made from a group III and a group V element, for example, GaAs) have nearly equal ionization rates for electrons and holes.

Using band-gap engineering, one can artificially tailor the ratio of the ionization coefficients and therefore reduce excess noise. Figure 1 illustrates three structures designed to achieve this goal (*17*). The superlattice APD (Fig. 1a) alternates layers of high- and low-gap materials and restricts ionizing collisions to the low-gap regions. Carriers accelerate and gain energy but do not ionize in wide-gap regions. On entering the next well a free electron gains enough energy from the conduction-band discontinuity ΔE_c to ionize. However, the valence-band discontinuity ΔE_v is not large enough to supply a similar energy boost to free holes. Thus electrons enter the well with a higher kinetic energy than holes, so that electrons ionize more efficiently than holes if $\Delta E_c > \Delta E_v$. This concept, proposed at the University of Illinois (*18*), was demonstrated by Capasso and coworkers (*19*). They obtained α/β of 7 to 8 in an $Al_{0.45}Ga_{0.55}As$ (500 Å)/GaAs (500 Å) multiquantum well APD with 50 periods, which represents an improvement of a factor of 3 to 4 over α/β in GaAs (= 2) (*19*).

A staircase APD (*17*), on the other hand, uses a superlattice of layers that are graded from low gap to high gap (Fig. 1b). Here, the band gap widens gradually in each layer but narrows abruptly at the layer interface. As in the earlier case, the band-gap difference is most visible in the conduction band, where the discontinuities form steps. As a reverse bias is applied, the sawtooth band diagram becomes a staircase. A free electron drifts toward the right in the graded layer but cannot ionize there, because the field is too low. However, the discontinuity furnishes all the energy an electron needs to ionize, so ionizing collisions occur only at the steps. Because the valence-band steps are of the wrong sign to enhance ionization and the electric field is too small to furnish the energy needed, holes do not ionize in this structure. The staircase APD is the solid-state analog of a photomultiplier, a type of vacuum tube detector with high internal amplification and negligible avalanche noise. As in a photomultiplier, the negligible avalanche noise of the staircase APD arises not only from the lack of feedback by ionizing holes but also from electrons ionizing at well-defined locations (the conduction band steps, which are equivalent to the photomultiplier dynodes) (*17*). This minimizes the intrinsic randomness of an avalanche. Such a structure can also operate at very low voltages ($\approx$6 V for a five-stage device with a gain of $\approx$32 and a conduction band discontinuity of $\approx$1 eV), a feature not present in conventional avalanche photodiodes. This structure has not been fabricated and represents a challenge for the MBE crystal grower; promising materials are HgCdTe/CdTe and certain III-V alloys.

Another device, the channeling APD (Fig. 1c), consists of alternated *p*- and *n*-layers of different band gap, with lateral *p*- and

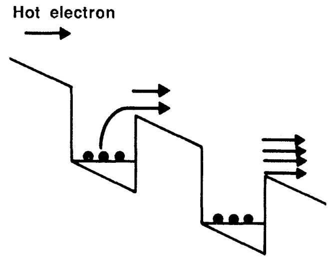

Fig. 2. Band diagram of impact-ionization across the band discontinuity of electrons stored in the quantum wells by hot carriers in the barriers. This phenomenon can also be used to implement a solid-state analog of a photomultiplier.

n-contacts (*20*). The energy band diagram of this device is three dimensional. Here, the band boundaries resemble two gutters separated by a space, which is the band gap. Channels (formed by the *pn* junction) run parallel to the layers. A periodic, transverse electric field (perpendicular to the layers) results from the alternated *npnp* layers, while an external field is applied parallel to the layers. The transverse field collects electrons in the low-gap *n*-layers, where they are channeled by the parallel electric field, so electrons impact-ionize in the low-gap *n*-layers. But the transverse field also causes holes created by electrons ionizing in the *n*-layers to transfer into the wide-gap *p*-layers before ionizing. Once they are there, holes cannot impact-ionize, because the band gap is too high to permit multiplication. The α/β ratio of this device is therefore very high and the avalanche noise very small. Channeling devices have novel applications in high-energy physics as solid-state drift chambers (*21*).

Another avalanche multiplication mechanism in superlattices suitable for a solid-state photomultiplier has been proposed (*22, 23*) and demonstrated (*23*) (Fig. 2). Hot carriers in the barrier layers collide with carriers confined or dynamically stored in the wells and impact-ionize them out across the band-edge discontinuity. In this ionization process only one type of carrier is created, so that positive feedback of impact-ionizing holes is eliminated. Thus a quiet avalanche with small excess noise as in a photomultiplier is possible. This effect has some conceptual similarities with the impact-ionization of deep levels, in that the quantum well may be treated as an artificial trap.

One application of band-gap engineering to devices other than detectors may be in the development of a faster transistor. Invented at Bell Laboratories in the late 1940's, the bipolar transistor consists of three layers: an emitter, a base, and a collector. A current injected in the base layer controls the flow of electrons from the emitter to the collector layer. In conventional bipolar transistors, the base has a uniform band gap but no electric field. Therefore, electrons traversing the base travel relatively slowly by diffusion.

One way to speed up electrons is to use a graded-gap material for the base. The gradual change in composition causes the conduction band in the base layer to "tilt" as if an electric field was present (Fig. 3). Electrons drift through the base much faster than in the conventional device. This concept was pioneered by Kroemer (*2*). Recently, AT&T Bell Laboratories demonstrated this concept in a phototransistor (*24*) and in a three-terminal bipolar transistor (*25*) grown by MBE. The graded-gap transistor had an AlGaAs emitter and a GaAs collector. Its *p*-type base, about 3000 Å thick, changed composition gradually, from the emitter at one end to the collector at the other. The grading gave the base an effective electric field of about 6 kV/cm. In initial tests, the device operated at frequencies up to 4 GHz with a d-c current gain greater than 1000. Direct velocity measurements showed that electrons in the graded base can travel up to ten times as fast as electrons in the base of an ungraded transistor (*3*). Scientists expect operating frequencies above 50 GHz from these graded transistors. A maximum oscillation frequency of 45 GHz has been recently demonstrated (*26*).

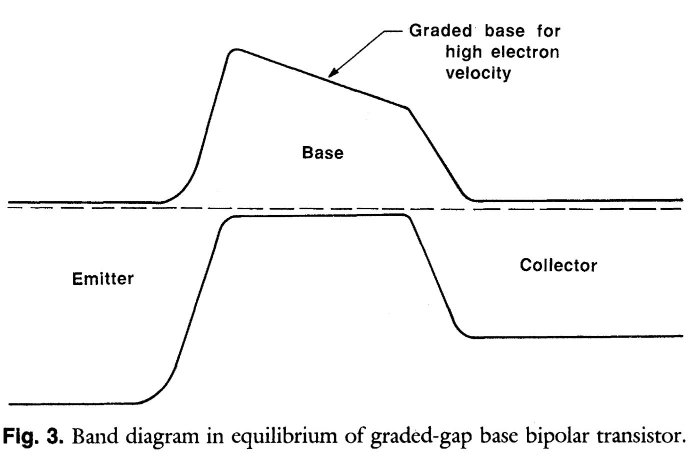

Fig. 3. Band diagram in equilibrium of graded-gap base bipolar transistor.

Tunneling Devices

The formation of quantum resonances in narrow potential wells has opened the door to interesting transport phenomena and device applications. Consider an undoped double barrier (for example, AlAs/GaAs/AlAs grown by MBE) sandwiched between two heavily doped contact layers. Figure 4a shows how tunneling occurs with applied d-c bias. Electrons originate near the Fermi level to the left of the first barrier and tunnel through the well. Resonant tunneling occurs when the energy of the injected carriers becomes equal to the energy of one of the levels in the well. Maxima occur in the overall transmission through the double barrier and in the current-voltage curves (*27*). This negative differential resistance may be useful in ultrahigh-frequency device applications. Sollner *et al.* recently reported resonant tunneling double-barrier oscillators operating at frequencies up to 35 GHz (*28*). The resonant tunneling effect is essentially equivalent to the resonant enhancement of the transmission in an optical Fabry-Perot interferometer, provided that scattering in the double barrier is negligible (that is, transport must be coherent).

Resonant tunneling transistors have been recently proposed. These have an *npn* bipolar transistor structure with a quantum well in the base region rather than a graded layer (*29*). Figure 4, b and c, shows the band diagrams of two types of resonant tunneling bipolar transistors under operating conditions. The voltage between the base-emitter junction is such that electrons in the emitter resonantly tunnel through one of the energy levels of the well and are collected by the reversed-biased base-collector junction. Only when such resonance conditions are satisifed can electrons injected from the emitter reach the collector and give rise to transistor action. A plot of the collector current versus the base-emitter bias voltage displays a series of peaks corresponding to the quantum levels of the well. Resonant tunneling is accomplished not by applying an electric field to the double barrier but by varying the energy of the incident electrons. Thus the symmetry of the double barrier is maintained, and coherent resonant tunneling should be achieved with near unity transmission at all resonances, as in a Fabry-Perot resonator. In the first structure (Fig. 4b), electrons are ballistically launched into the quantum well by the conduction-band discontinuity at the base-emitter interface. In the second one (Fig. 4c), a parabolic quantum well is placed in the base. Such wells have been recently grown by MBE and exhibited the expected equal spacing of the energy levels (*30*).

The device in Fig. 4c is the exact electronic equivalent of a Fabry-Perot interferometer. By appropriately connecting the resonant tunneling transistor to a resistive load and a voltage supply, one can produce a device with N stable states, where N is the number of

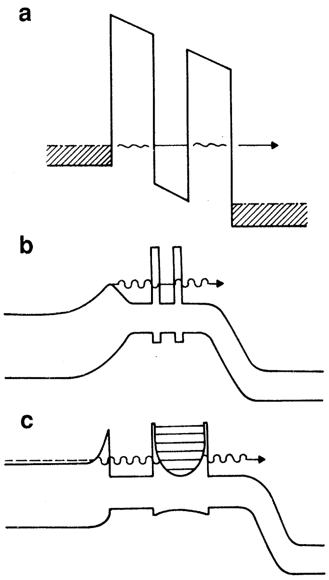

Fig. 4. Resonant tunneling (RT) heterostructures. (**a**) RT through a double barrier; (**b**) RT bipolar transistor with near ballistic injection under operating conditions; and (**c**) RT bipolar transistor with parabolic quantum well for multiple-valued logic applications.

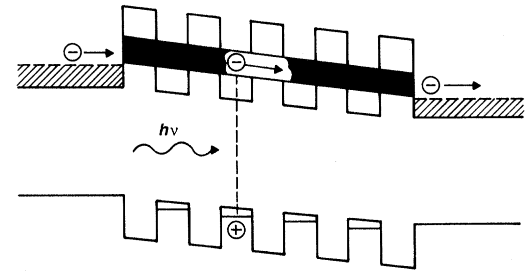

Fig. 5. Band diagram of a superlattice photoconductor, which shows the effective mass filtering mechanism.

resonant peaks (*29*). In this configuration, the device serves as an N-state memory element (with N as high as ≈ 8), providing the possibility of extremely high density data storage. Memories of this sort and other multiple-valued logic circuits based on multiple negative resistance, such as counters, multipliers and dividers, have been of interest for quite some time. However, since no physical device exhibiting multiple-valued negative differential resistance previously existed, such circuits were possible only with combinations of binary devices. This resulted in complex configurations with reduced density and speed. Because resonant tunneling transistors allow multiple-valued differential resistance in a single physical element, they have tremendous potential. Recently Capasso *et al.* demonstrated the first resonant tunneling bipolar transistor (*31*). These devices operate at room temperature and exhibit both negative transconductance and negative conductance in the common emitter configuration. The operating principle and overall structure of this device are similar to those of the resonant tunneling transistors previously proposed (Fig. 4b) (*29*). Nevertheless, the essential difference is that in the implemented resonant tunneling transistor (*31*) electrons are injected thermally into the quantum well, rather than quasi-ballistically. This makes the operation of the device much less critical, and allows operation at room temperature.

Tunneling in superlattices is also of considerable physical and practical interest. As pointed out by Capasso *et al.* (*32*), a superlattice can act as an effective mass filter (Fig. 5). Since the tunneling probability increases exponentially with decreasing effective mass, electrons are transported through a superlattice more readily than the heavy holes as long as the valence-band discontinuity is not negligible compared to the conduction-band discontinuity. Effective mass filtering is the basis of tunnel-photoconductivity, recently discovered at Bell Laboratories (*32, 33*). In a classical photoconductor, photogenerated electrons and the electrons injected from the ohmic contacts can be viewed as moving through the semiconductor and around the circuit until they recombine with the slowly moving photogenerated holes. This produces a current gain whose value is given by the ratio of electron-hole pair lifetime to the electron transit time (*34*). In a superlattice, photogenerated heavy holes remain localized in the wells as a result of the negligible tunneling probability. Electron states tend to be extended, because of the small electron effective mass ($\approx 1/10$ of the heavy hole mass) and the ultrathin barriers. These extended states form a band referred to as a miniband. Thus, photoelectrons will be transported by band-type conduction. Since carrier mobility in the miniband depends exponentially on the superlattice barrier thickness (an effect caused by tunneling), the electron transit time, the photoconductive gain, and the gain-bandwidth product can be artificially tuned over a wide range. This offers a great versatility in device design, which is not available in standard photoconductors. High-performance infrared photoconductors that utilize effective mass filtering were recently demonstrated (*32*). The MBE-grown devices consisted of 100 periods of AlInAs (35 Å)/GaInAs (35 Å) between two contact layers. These devices responded to wavelengths in the 1.6- to 1.0-μm region and exhibited high current gain (up to 2×10^4) at low voltage (≤ 1 V) with response times in the range of 10^{-4} second. The low bias operation reduces device noise to only $\approx 3 \times 10^{-14}$ $W/Hz^{1/2}$.

In superlattices with relatively thick barriers (≥ 100 Å) the electron states also become localized, and one can observe sequential resonant tunneling (Fig. 6) (*35*). Electrons tunnel from the ground state of a given well into the excited states of the adjacent well. This is followed by intrawell energy relaxation (mostly nonradiative) to the ground state. This process is repeated many times to produce a typical cascade process through the whole superlattice (Fig. 6a). The observation of this effect (*35*) has led to many exciting device possibilities. One is a solid-state infrared laser which emits radiation in the range from 5 to 250 μm (depending on the well thickness), as originally proposed by Kazarinov and Suris (*36*). The laser transition occurs between the third and second states of the quantum

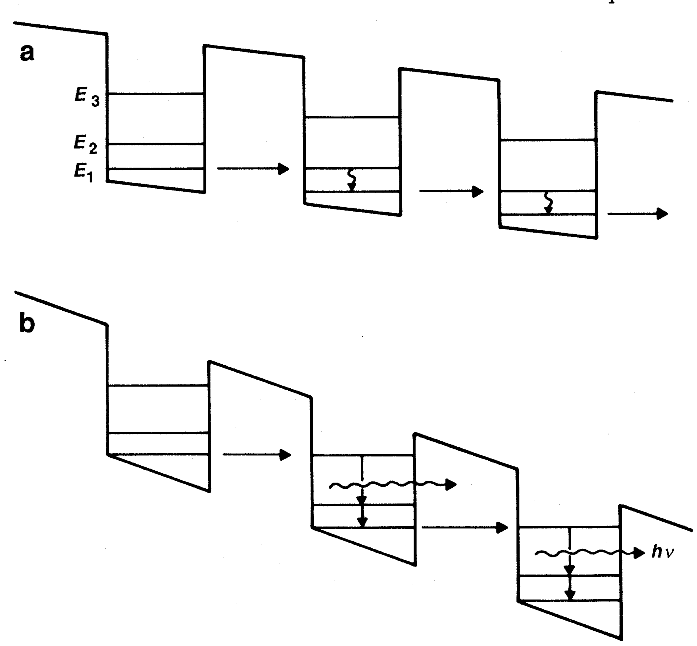

Fig. 6. (**a**) Sequential resonant tunneling through a superlattice. Intrawell transitions occur primarily by nonradiative relaxation. (**b**) Sequential resonant tunneling laser.

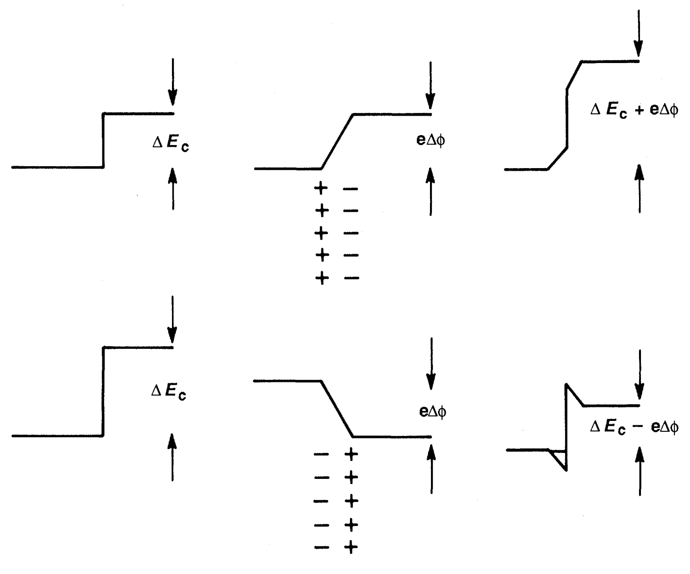

Fig. 7. Tunable band discontinuities formed from doping-interface dipoles. (**Top**) The conduction band discontinuity is increased. (**Bottom**) Interchange of the acceptor and donor sheets reduces the band discontinuity. Tunneling through the spike and size quantization in the triangular well plays a key role in this reduction.

wells after a population inversion has been achieved between these levels (Fig. 6b). Another intriguing application is the generation of sub-Poisson light, that is, radiation with sub-shot noise properties (*37*).

The Ultimate Band-Gap Engineering: Tunable Band Discontinuities

The reader has probably realized the importance of band discontinuities in the design of band gap–engineered structures and quantum devices. The ability to artificially control such discontinuities would add a powerful degree of freedom in the design of materials and devices. Two methods have been successfully demonstrated independently by groups at Bell Laboratories (*38*) and the University of Wisconsin (*39*). The Bell Laboratories approach (Fig. 7) consists of the incorporation by MBE of ultrathin (≤ 50 Å) ionized donor and acceptor sheets within a few tens of angstroms from the heterojunction interface (planar doping). The electrostatic potential of this "doping interface dipole" is added to or subtracted from the dipole potential of the discontinuity. Since the separation between the charge sheets is on the order of or smaller than the carrier de Broglie wavelength, electrons crossing the interface "see" a new band discontinuity $\Delta E_c \pm e\Delta\phi$, where $\Delta\phi$ is the potential of the double layer. Using this technique, Capasso *et al.* demonstrated an artificial reduction of the conduction band discontinuity of the order of 0.1 eV in an $Al_{0.25}Ga_{0.75}As$/GaAs heterojunction (*38*). This lowering of the barrier produced an enhancement (by one order of magnitude) of the collection efficiency of photocarriers across the heterojunction as compared to identical heterojunctions without doping interface dipoles (*38*). On the other hand, Margaritondo and co-workers used ultrathin interlayers grown in the vicinity of the heterojunction (*39*). These interlayers also alter the band discontinuities. These techniques of modifying band offsets offer tremendous potential for heterojunction devices. The performance of many of these devices depends exponentially on band discontinuities. Thus artificial variations of these quantities by 1 or 2 kT (thermal energy, where k is Boltzmann's constant and T is temperature) can significantly alter that performance.

The key in this approach to designing microstructures and devices is the ability to model the energy band diagrams of semiconductor structures. With these models, scientists can visualize the behavior of electrons and holes in a device. Variable gap materials, superlattices, band discontinuities, and doping variations can be used alone or in combination to modify the energy bands almost arbitrarily and to tailor these bands for a specific application.

REFERENCES AND NOTES

1. W. Shockley, U.S. Patent 2 569 347 (1951).
2. H. Kroemer, *RCA Rev.* **18**, 332 (1957).
3. For recent reviews on band-gap engineering see F. Capasso, in *Gallium Arsenide Technology*, D. K. Ferry, Ed. (Sams, Indianapolis, 1985), chap. 8; F. Capasso, in *Picosecond Electronics and Optoelectronics*, G. Mourou, D. M. Bloom, C. H. Lee, Eds. (Springer-Verlag, Berlin, 1985), p. 112.
4. H. Kroemer, *Proc. IEEE* **51**, 1782 (1963).
5. Zh. I. Alferov *et al.*, *Sov. Phys. Semicond.* **4**, 1573 (1971) [translated from *Fiz. Tekh. Pouprovodn.* **4**, 1826 (1970)]; I. Hayashi, M. B. Panish, P. W. Foy, S. Sumski, *Appl. Phys. Lett.* **17**, 109 (1970).
6. A. Y. Cho and J. R. Arthur, *Progress in Solid-State Chemistry*, J. O. McCaldin and G. Somorjai, Eds. (Pergamon, New York, 1975), vol. 10, p. 157; M. B. Panish, *Science* **208**, 916 (1980).
7. N. Holonyak, R. M. Kolbas, R. D. Dupuis, P. D. Dapkus, *IEEE J. Quantum Electron.* **QE-16**, 170 (1980).
8. L. Esaki and R. Tsu, *IBM J. Res. Dev.* **14**, 61 (1970).
9. H. M. Manasevit, *Appl. Phys. Lett.* **12**, 156 (1969); R. D. Dupuis, *Science* **226**, 623 (1984).
10. G. Döhler, *J. Vac. Sci. Technol.* **B1**, 278 (1983).
11. F. Capasso, S. Luryi, W. T. Tsang, C. G. Bethea, B. F. Levine, *Phys. Rev. Lett.* **51**, 2318 (1983).
12. R. Dingle, H. L. Störmer, A. C. Gossard, W. Wiegmann, *Appl. Phys. Lett.* **33**, 665 (1978).
13. H. L. Störmer, R. Dingle, A. C. Gossard, W. Wiegmann, M. D. Sturge, *Solid State Commun.* **29**, 705 (1979); R. Dingle, A. C. Gossard, H. L. Störmer, U.S. Patent 4 194 935 (1980); T. Mimura, S. Hiyamizu, T. Fuji, K. Nanbu, *Jpn. J. Appl. Phys.* **19**, L125 (1980).
14. For strained layer superlattices in III-V materials, see G. C. Osbourn, *J. Vac. Sci. Technol.* **21**, 469 (1982); for Ge-Si strained layer superlattices, see J. C. Bean, *Science* **230**, 127 (1985).
15. J. M. Woodall, *Science* **208**, 908 (1980).
16. V. Narayanamurti, *Phys. Today* **37** (no. 6), 24 (1984).
17. F. Capasso, W. T. Tsang, G. F. Williams, *IEEE Trans. Electron Devices* **ED-30**, 381 (1983).
18. R. Chin, N. Holonyak, G. E. Stillman, J. Y. Tang, K. Hess, *Electron. Lett.* **40**, 38 (1982).
19. F. Capasso, W. T. Tsang, A. L. Hutchinson, G. F. Williams, *Appl. Phys. Lett.* **40**, 38 (1982).
20. F. Capasso, *IEEE Trans. Electron Dev.* **ED-29**, 1388 (1982).
21. E. Gatti and P. Rehak, *Nucl. Instrum. Methods* **225**, 608 (1984).
22. S. L. Chuang and K. Hess, *J. Appl. Phys.* **59**, 2885 (1986).
23. F. Capasso *et al.*, *Appl. Phys. Lett.* **48**, 1294 (1986).
24. F. Capasso, W. T. Tsang, C. G. Bethea, A. L. Hutchinson, B. F. Levine, *ibid.* **42**, 93 (1983).
25. J. R. Hayes, F. Capasso, A. C. Gossard, R. J. Malik, W. Wiegmann. *Electron. Lett.* **19**, 818 (1983); R. J. Malik *et al.*, *Appl. Phys. Lett.* **46**, 600 (1985).
26. G. J. Sullivan, P. M. Asbeck, M. F. Chang, D. L. Miller, K. C. Wang, paper III A-6, Technical Digest of the 44th Annual Device Research Conference, Amherst, MA, 23 to 25 June 1986.
27. L. L. Chang, L. Esaki, R. Tsu, *Appl. Phys. Lett.* **24**, 593 (1974). For a recent review on resonant tunneling in heterostructures, see F. Capasso, K. Mohammed, A. Y. Cho., *IEEE J. Quantum Electron.* **QE-22**, 1853 (1986).
28. T. C. L. G. Sollner, P. E. Tannewald, D. D. Peck, W. D. Goodhue, *Appl. Phys. Lett.* **45**, 1319 (1984).
29. F. Capasso and R. A. Kiehl, *J. Appl. Phys.* **58**, 1366 (1985). A unipolar resonant tunneling transistor with a quantum well in the emitter was demonstrated shortly hereafter by N. Yokoyama, K. Inamura, S. Muto, S. Hiyamizu, and H. Nishi [*Jpn. J. Appl. Phys.* **24**, L853 (1985)].
30. R. C. Miller, D. A. Kleinmann, A. C. Gossard, O. Munteanu, *Phys. Rev. B* **29**, 3740 (1984).
31. F. Capasso, S. Sen, A. C. Gossard, A. L. Hutchinson, J. H. English, *IEEE Electron. Dev. Lett.* **EDL7**, 573 (1986).
32. F. Capasso, K. Mohammed, A. Y. Cho, R. Hull, A. L. Hutchinson, *Appl. Phys. Lett.* **47**, 420 (1985).
33. ———, *Phys. Rev. Lett.* **55**, 1152 (1985).
34. A. Rose, *Concepts in Photoconductivity and Allied Problems* (Wiley, New York, 1963).
35. F. Capasso, K. Mohammed, A. Y. Cho, *Appl. Phys. Lett.* **48**, 478 (1986).
36. R. F. Kazarinov and R. A. Suris, *Sov. Phys. Semicond.* **5**, 707 (1971) [translated from *Fiz. Tech. Pouprovdn.* **5**, 797 (1971)].
37. F. Capasso and M. C. Teich, *Phys. Rev. Lett.* **57**, 1417 (1986).
38. F. Capasso, A. Y. Cho, K. Mohammed, P. W. Foy, *Appl. Phys. Lett.* **46**, 664 (1985); *J. Vac. Sci. Technol.* **B3**, 1245 (1985).
39. D. W. Niles, G. Margaritondo, P. Perfetti, C. Quaresima, M. Capozi, *Appl. Phys. Lett.* **47**, 1092 (1985); P. Perfetti *et al.*, *Phys. Rev. Lett.* **57**, 2065 (1986).